Atmospheric Research 199 (2018) 54–61

Contents lists available at ScienceDirect

Atmospheric Research

journal homepage: www.elsevier.com/locate/atmosres

Tropical echo-top height for precipitating clouds observed by multiple active instruments aboard satellites

Yilun Chen, Yunfei Fu*

School of Earth and Space Sciences, University of Science and Technology of China, Hefei 230026, China

ARTICLE INFO

Keywords:
Echo-top height
PR
CPR
CALIOP
Radiative forcing

ABSTRACT

The echo-top height observed by the Tropical Rainfall Measuring Mission (TRMM) precipitation radar (PR) has been used by some studies as an approximate calculation of the precipitating-cloud-top height to simulate radiative forcing or to identify overshooting convection. However, due to the low sensitivity (~17 dBZ) of PR, the PR-echo-top height is lower than the actual precipitating-cloud-top height. Here, the echo-top heights of the tropical precipitating cloud detected by PR, the Cloud Profiling Radar (CPR), and the Cloud-Aerosol Lidar with Orthogonal Polarization (CALIOP) were investigated to evaluate the underestimation of the PR-echo-top height to the actual precipitating-cloud-top height. The results show that there were significant spatial variations in the underestimates of precipitating-cloud-top height by PR. The model simulation showed that these underestimates led to an underestimation of the radiative forcing of the Earth system, the relative error of which was ~10% with 1-km underestimation and ~20% to 80% with 7-km underestimation when the cloud optical thickness was fixed to 10. Therefore, the underestimates of precipitating-cloud-top height by PR should be taken into consideration when using PR-echo-top height.

1. Introduction

The echo-top height observed by the Tropical Rainfall Measuring Mission (TRMM) precipitation radar (PR) reflects the "precipitation-top height", which is commonly used to estimate rain rate or assess the magnitude of convection development (Hamada et al. 2015; Shige and Kummerow 2016). In some studies, the PR-echo-top and PR-echo-bottom heights have been subtracted to calculate the thickness of the anvil (Schumacher and Houze 2006; Li and Schumacher 2011; Yang et al. 2015). The PR-echo-top height, assumed to approximate the cloud-top height, has been compared with the tropopause to identify overshooting (tropopause-penetrating) convection (Liu and Zipser 2005; Xian and Fu 2015). Furthermore, the PR-echo-top height has been taken as an input parameter in some models to simulate the heating profile or radiative forcing (Lau and Wu 2010; Yang et al. 2017). It also has been used to identify precipitation type (deep weak convective precipitation, shallow precipitation, and deep strong convective precipitation) over the Tibetan Plateau (Fu et al. 2016).

However, due to the low sensitivity (~17 dBZ) of the PR (Schumacher and Houze 2003), its echo-top height is lower than the actual precipitating-cloud-top height, which can lead to the miscalculation of the anvil, the overshooting convection, and the radiative forcing. Based on the assumption that the infrared brightness temperature represents the cloud-top height, Lau and Wu (2011) compared the PR-echo-top height with the infrared brightness temperature observed by the TRMM Visible and Infrared Scanner (VIRS). They found that heavy rain was associated with the cold infrared brightness temperature and elevated PR-echo-top heights, and light rain was associated with the warm infrared brightness temperature and low PR-echo-top heights, respectively, whereas intermediate rain (25th to 75th percentile) contributed to a wide range of infrared brightness temperature and PR-echo-top heights. Recently, Chen and Fu (2017) concluded that the beam-filling problem also resulted in a difference (~5 to 15 K) in the infrared brightness temperature within each warm-rain-PR pixel. These studies indicate that the infrared brightness temperature of VIRS does not fully represent the actual cloud-top height.

Therefore, the accurate assessment of actual cloud-top height relies on active sensors with high sensitivity, such as, LIDAR or Cloud Profiling Radar (CPR). Casey et al. (2007) investigated the cloud-top difference between the TRMM PR and Geoscience Laser Altimeter System (GLAS) using coincident scans (1279 pixels in total), finding that the echo-top height peaked at 5 km for PR and 15–16 km for GLAS. Li and Schumacher (2011) compared a coincident scan of PR and CloudSat CPR, concluding that PR underestimated the anvil tops from 1 to 10 km with an average of 5 km, and some of the anvil samples were missed by PR. However, these studies lacked a sufficient number of

* Corresponding author.
E-mail address: fyf@ustc.edu.cn (Y. Fu).

http://dx.doi.org/10.1016/j.atmosres.2017.08.008
Received 22 May 2017; Received in revised form 4 August 2017; Accepted 8 August 2017
Available online 09 August 2017

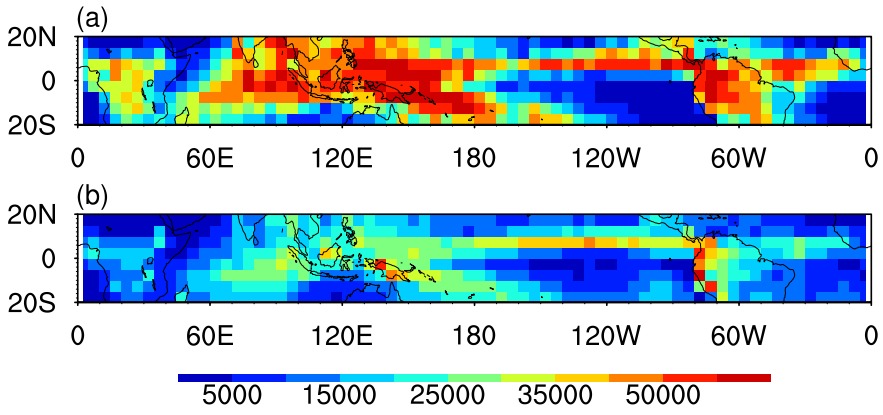

Fig. 1. Distributions of the total number of sample for precipitating cloud observed by (a) PR, (b) CPR from 13th June 2006 to 31st December 2010. Please note that PR observations were only used for time periods from 0100 to 0200 and 1300 to 1400 local time since CPR observes at approximately 1330 and 0130 LST.

samples and therefore it is difficult to assess the regional differences.

The cloud-top height of the precipitating cloud has an important effect on cloud morphology, particle size, radiative forcing, and liquid water content (Rangno and Hobbs 2005). Understanding the difference between the PR-echo-top height and the actual precipitating-cloud-top height will provide an accurate input for model simulation to effectively reduce the error in estimating these physical parameters. Although some studies have measured the echo-top height of the CloudSat CPR or TRMM PR alone (Riley and Mapes 2009; Fu et al. 2012; Chen et al. 2016; Chen et al. 2017), due to the lack of a uniform standard (CPR was generally used to study the "cloud" rather than the "precipitating cloud", and PR was generally used to study the "precipitation") or lack of sufficient samples (Casey et al. 2007; Li and Schumacher 2011), the tropics-wide difference between PR-echo-top height and actual precipitating-cloud-top height is not yet understood. In this study, TRMM PR reflectivity and CloudSat/CALIPSO L2 data were used to compare the echo-top height difference of the tropical precipitating clouds and evaluate the impact of underestimating the cloud-top height on radiative forcing estimates.

2. Data and method

The PR operates at 13.8 GHz with 5-km horizontal and 250-m vertical resolution after a 2001 boost (Kummerow et al. 1998). As members of the A-Train constellation, CloudSat and CALIPSO were launched in 2006 using a sun-synchronous 705-km-altitude orbit with 1330 and 0130 LST (Local Standard Time) crossings of the equator. The CPR onboard CloudSat operates at 94 GHz with 240-m vertical resolution and − 30-dBZ sensitivity, which can observe 2D (cross-track and vertical) cloud structure (Stephens et al. 2008). The minimum detectable reflectivity was also reported as − 28 dBZ in some publications (Im et al. 2005). The Cloud-Aerosol Lidar with Orthogonal Polarization (CALIOP) onboard CALIPSO is a near-nadir viewing two-wavelength polarization-sensitive LIDAR that can more effectively detect thin clouds, compared with CPR or other passive remote sensors, to accurately obtain cloud-top height. For example, Liu et al. (2016) found that CPR missed 24–36% oceanic thin warm clouds (optical thickness < 4) after comparing with CALIOP. The CALIOP provides 532 and 1064 nm attenuated backscatter profiles at the horizontal resolution of 1 km (333 m) and the vertical resolution of 60 m (30 m) at altitudes of 8.3 to 20.2 km (− 0.5 to 8.3 km) (Winker et al. 2009).

We used PR 2A25 V7 data to provide reflectivity and 3D rain rate (Iguchi et al. 2000). A precipitating cloud was defined by a near-surface rain rate > 0.1 mm/h and a maximum reflectivity not < 17 dBZ. The PR-echo-top height was defined as the first layer from top to ground with a minimum echo exceeding 17 dBZ.

The standard product 2B-GEOPROF provides CPR reflectivity and a cloud mask. The "cloud mask" contains values between 0 and 40, and increasing values indicate a reduced probability of a false detection (Marchand et al. 2008). The 2B-CLDCLASS product provides a "precipitation flag" for each pixel using temperature and reflectivity thresholds, including "no precipitation", "liquid precipitation", "solid precipitation", and "possible drizzle" (Sassen and Wang 2007). Precipitating cloud observed by CPR was defined by pixels with a precipitation flag of "liquid precipitation" or "solid precipitation". The highest layer with reflectivity greater than − 30 dBZ and a cloud mask not < 20 was defined as the CPR-echo-top height.

The 2B-GEOPROF-LIDAR is a collaborative product of CPR and CALIOP, which integrates CALIOP pixels to CPR pixels and provides the LIDAR cloud fraction within a CPR footprint (Mace and Zhang 2014). The CALIOP-echo-top height was defined as the highest layer with a cloud fraction > 50%. Because of the sensitivity and strong attenuation of CALIOP, the precipitating flag identified by CPR was integrated with CALIOP. In general, the CALIOP-echo-top and CPR-echo-top heights represent the actual cloud-top height. Only certain high thin cirrus and shallow continental stratus will be below the detection threshold of the CPR, and CALIOP can identify them correctly.

To reduce the influence of interannual variability on the results, we chose to study the period during which PR, CPR, and CALIOP were all working normally (13th June 2006 to 31st December 2010). Because CPR and CALIOP always observe at approximately 1330 and 0130 LST, we only counted the PR pixels from 0100 to 0200 LST, and 1300 to 1400 LST, to avoid the error caused by the diurnal variation of the precipitating cloud. Based on the above restrictions, the number of precipitating cloud samples observed by the PR and CPR showed similar patterns (Fig. 1), and the number of samples in the 5 × 5° grid was sufficient for statistical analysis. Overall, CPR and PR both observed more precipitating cloud samples over the Central Africa, Indonesia, Argentina, central Indian Ocean, and Intertropical Convergence Zone, whereas the less samples occurred in southeast and northeast Pacific, and African coast. Some discrepancies occurred in part of the south Atlantic, and east Pacific near the South America, where the precipitating cloud samples observed by CPR were even greater than the PR precipitating cloud samples. Please note that time matching between PR and CPR (near-coincident PR-CPR-CALIOP dataset) was not used in this part and later statistical analysis because of the rare near-coincident samples.

SBDART (Santa Barbara DISORT Atmospheric Radiative Transfer) was used to estimate the effect of cloud-top-height underestimation on radiative forcing using the tropical standard atmospheric profile (Ricchiazzi et al. 1998). This model is scripted in the FORTRAN 77 language and designed for the analysis of radiative transfer problems in satellite remote sensing (Fu 2014) and atmospheric energy budget (Fu et al. 2017). The SBDART utilizes the file named INPUT to handle the user inputs. Users can define tens of interesting parameters and output options including atmospheric profiles, aerosols, surfaces and clouds. If the parameters are not specified by the users in INPUT file, these parameters will be determined as default settings. Because the

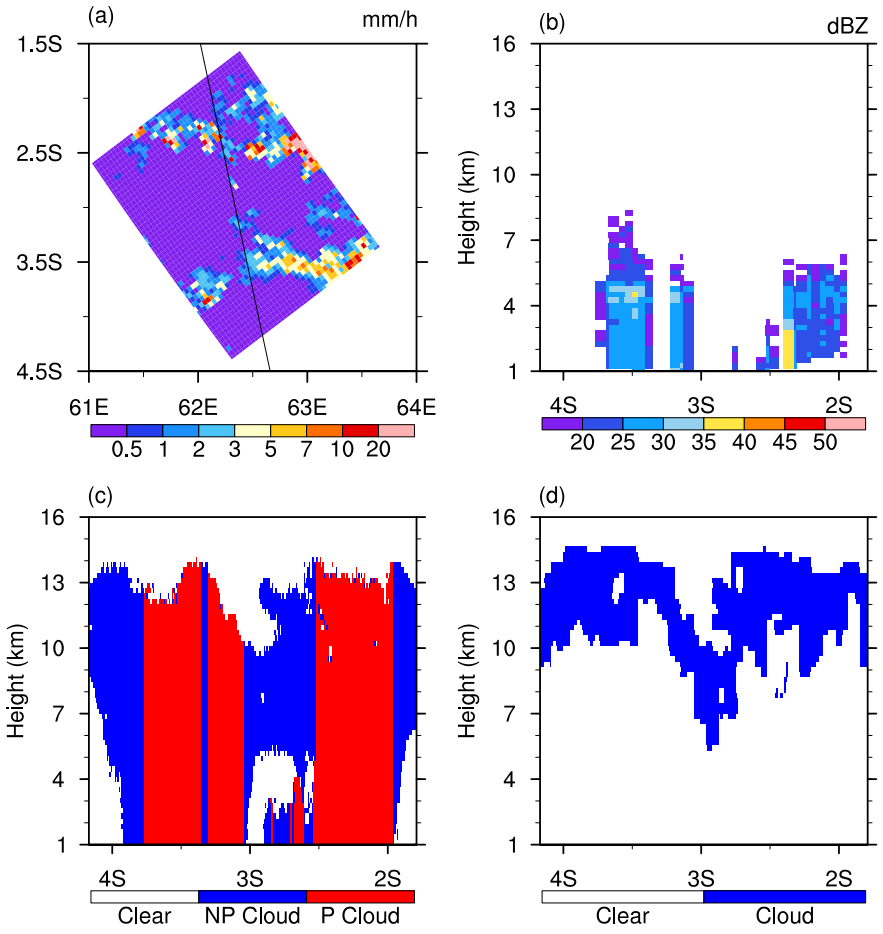

Fig. 2. An example crossover match from the central Indian Ocean on 28th January 2007 by PR, CPR, and CALIOP within one-minute intervals. (a) PR near-surface rain rate (base map) with CPR track (black line). Vertical cross sections of (b) PR reflectivity, (c) CPR precipitating cloud, and (d) CALIOP cloud.

difference of cloud-top height was the focus of this study, other inputs to SBDART were set to default values to avoid introducing further errors. Input settings were introduced in detail in Discussion Section.

3. Results

3.1. Sample analysis

Although TRMM and CloudSat/CALIPSO run on completely different orbits, there were some quasi-simultaneous observations in the long time period from 2006 to 2010. Given these coincident scans of PR, CPR and CALIOP could be used more intuitively to understand the differences in the multi-sensor observations to avoid blind statistics. Fig. 2 shows an example crossover match from the central Indian Ocean on 28th January 2007. CPR and CALIOP scanned over the Fig. 2a area from south to north (the black line in Fig. 2a), and PR scanned from southwest to northeast (the regional precipitation rate estimate in Fig. 2a was provided by PR). CPR and CALIOP were approximately 1 min in front of PR, which could be considered as a quasi-simultaneous observation. The observed results were as expected. The three main precipitating clouds detected by PR at 3.6 °S, 3.2 °S, and 2.3 °S were all detected by the CPR, which indicates that the two sensors were consistent in their detection of precipitating cloud. Therefore, the independent statistics based on the precipitating cloud over this long time period by CPR and PR could be used to analyze the underestimation of precipitating-cloud-top height by PR. For the three main precipitating clouds, the PR-echo-top heights were 6–8 km, 5–6 km, and approximately 6 km, whereas the CPR-echo-top heights were 12–14 km, 11–14 km, and 13 km. The CALIOP-echo-top height was the highest, up to 15 km. In the gaps among the three main precipitating clouds, CPR and CALIOP detected no-precipitating clouds with a thickness of 4–6 km, which may have been the anvils completely missed by PR. The CPR also detected "possible drizzle" near 3.3 °S and 3.9 °S, which was missed by PR. The above results were due to the large differences in the sensitivity of the sensors. However, the focus of this study was the underestimation of the precipitating-cloud-top height observed by PR, therefore, only the precipitating clouds detected by CPR were incorporated into our statistics to calculate actual cloud-top height.

3.2. Statistical analysis

Based on the coincident scan example in Fig. 2 and the precipitating cloud samples detected by PR and CPR presented in Section 2, we established a uniform standard for the precipitating cloud from PR and CPR to calculate regional statistics. Fig. 3 shows the echo-top heights of the tropical precipitating cloud observed by PR, CPR, and CALIOP. The PR-echo-top height was distributed at 6–9 km over land, and 2–7 km over ocean, which is consistent with Chen et al. (2016). The land-ocean difference was obvious, which was due to the stronger heating effect and the higher terrain of the land than the ocean. Specifically, the average PR-echo-top height in central Africa was up to 9 km, while it was only 2 km in the eastern Pacific. The CALIOP-echo-top height in central Africa, Indonesia, and the American continent could be > 10 km, or more than the PR-echo-top height. These areas are usually convective with a high incidence of overshooting convention (Xian and Fu 2015). Also in the South Pacific Convergence Zone and the Intertropical Convergence Zone, some high cloud tops (11 to 15 km) were observed by CALIOP because of the convergence of the trade winds. Interestingly, the average CPR-echo-top height in these areas was approximately 13 km, and the CALIOP-echo-top height was > 16 km,

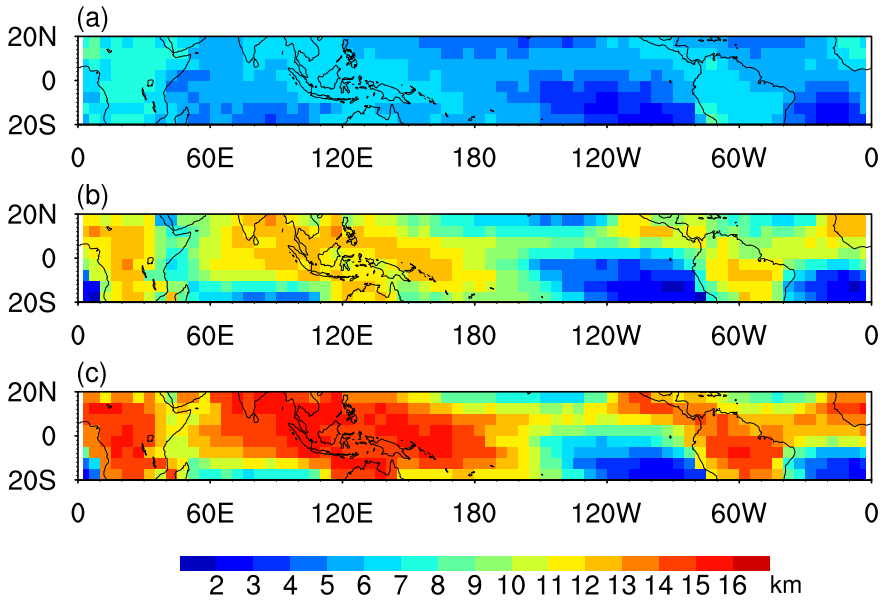

Fig. 3. Echo-top height of tropical precipitating cloud observed by (a) PR, (b) CPR, and (c) CALIOP from 13th June 2006 to 31st December 2010.

which indicates that many of the convective activities in these areas were not high (6–9 km) based on PR observations. However, the actual cloud (hydrometeor) may have affected the tropopause, transporting the water vapor and chemical constituents from the troposphere to the stratosphere. Thus, conventional studies using PR-echo-top height, such as Liu and Zipser (2005), may have greatly underestimated the proportion of overshooting convection. In the Eastern Pacific and the South Atlantic, the echo-top heights detected by PR, CPR, and CALIOP were all low; most of them lower than the freezing layer. These findings are consistent with earlier studies, which found that “warm rain” dominated by > 50% over these regions (Liu and Zipser 2009). The high frequency of shallow precipitation is a possible reason for this relatively low echo-top height (Chen et al. 2016). The echo-top heights observed over these low-echo-top regions by CPR and CALIOP were slightly lower than the PR-echo-top height, which may have been due to the mixing of the low-layer (< 1 km) echo with the surface echo, causing PR to miss some low level precipitating clouds. Another possible explanation is the beam-filling problem. That is, PR footprint (~5 km) is larger than CPR footprint (~1.7 km), which may lead to the smoother PR-echo-top height and wider distribution of CPR-cloud-top height.

Probability Distribution Functions (PDFs) were used to quantify the differences in PR, CPR, and CALIOP for echo-top observations. Because all the samples in the tropics were used, the distributions of the echo-top height in Fig. 4 are much smoother than the grid statistics in Fig. 3. The echo-top height of the PR-precipitating cloud over tropical land peaked at 5.5 km, as well as at the freezing layer in the tropics. When the echo-top was higher than the freezing layer, the precipitation particles were gradually converted from liquid to solid. However, the echo-top heights of precipitating cloud observed by CPR and CALIOP were significantly different from that measured by PR. At 2 km or less, the CPR detected more low-echo-top clouds than PR, as described above, which may have been missed by PR because of mixing with the surface echo. The echo-top heights of CPR and CALIOP had approximately uniform distributions between 3 and 10 km. The CPR-echo-top height peaked at 13.5 km, and the CALIOP-echo-top height peaked at 16 km, which was located in the tropical tropopause layer usually from 14 to 18.5 km (Fueglistaler et al. 2009). After reaching the peak, the PDFs of CPR and CALIOP decreased abruptly as the height increased, with only a few breaking through the upper bound of the tropical tropopause layer. Without considering the regional differences, the peaks of the CPR and CALIOP were approximately 10 km higher than the peak of the PR. This suggests that the overshooting convection identified by the PR may need to be redefined.

Over the ocean, the PR-echo-top height showed a bimodal distribution. In addition to a peak located at the freezing layer, there was also a peak near 3 km, which was the trade stable layer (Johnson et al. 1999). Because the trade clouds were usually relatively thin, the echo-top heights of the CPR and CALIOP also peaked at this altitude. Both CPR and CALIOP had peaks at the height of the tropopause layer, although weaker than those for the land, indicating a lower proportion of deep convective precipitating clouds over the ocean.

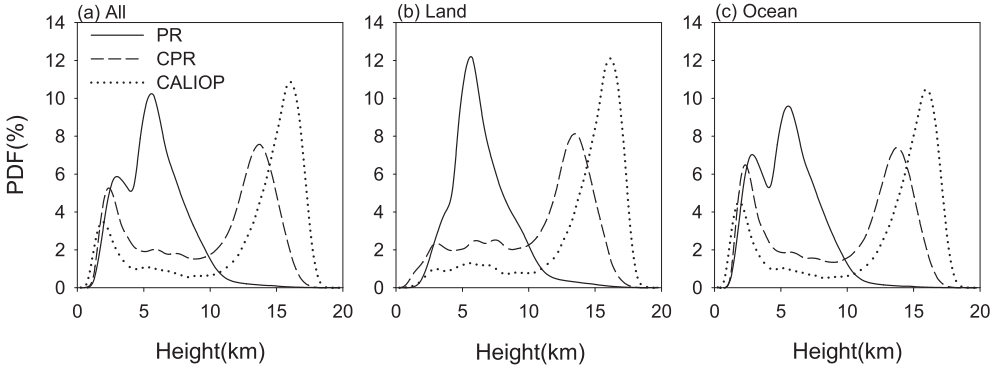

Fig. 4. Probability Distribution Functions (PDFs) of the echo-top height for precipitating cloud observed by PR, CPR, and CALIOP over (a) the tropics, (b) tropical land, and (c) the tropical ocean.

4. Discussion

Some previous studies have used PR-echo-top height as the precipitating-cloud-top height to simulate the radiative forcing of the precipitating cloud. Based on the above findings, the echo-top height observed by PR was substantially lower by 10 km compared with the actual cloud-top height, except for trade wind cumulus. Due to the lack of a suitable standard for comparison, it is difficult to determine using the conventional method how much PR underestimates the cloud-top height and how much the underestimated cloud-top height impacts on the radiative forcing estimate. In this study, SBDART was used to simulate the effects of the underestimated cloud-top height on radiative forcing in different underlying surfaces and different solar zenith angles. Please note that only precipitating clouds were discussed in this part. The cloud optical thickness (τ) had a large effect on the radiative forcing. We therefore controlled this variable τ and set it to 10, 30, 50, 70, and 90, respectively. We also assumed that the cloud-top height was located from 6 to 14 km to test its sensitivity to radiative forcing. Because the radiative differences between the different cloud-top heights were our main interest instead of the radiation fluxes of a specific cloud, the atmospheric profile and the cloud-bottom height (fixed to 3 km) should be fixed to constant value to avoid introducing additional errors.

Radiative forcing was defined as $RF = (F_{cloud}^{\downarrow} - F_{cloud}^{\uparrow}) - (F_{clear}^{\downarrow} - F_{clear}^{\uparrow})$, which is the difference in net radiation between cloudy and clear-sky conditions. The schematic diagram (Fig. 5) illustrates the above parameters in detail. Fig. 6 shows the simulation results based on the above inputs. The positive value of the abscissa in Fig. 6 indicates that the Earth system received more net radiation during cloudy skies than clear skies, and the positive value of the ordinate was for the RF on the Earth's surface. In theory, clouds reflect incoming solar radiation (cooling the Earth system), and reduce outgoing infrared radiation (warming the system) (Baker 1997). Fig. 6a shows that the presence of the cloud greatly reduced the net radiation received by the Earth system and the ground when the surface consisted of vegetation and the solar zenith angle was 0° (solar radiation of approximately 1370 W/m^2). For example, compared with clear sky, the Earth system received less net radiation by 220.4 W/m^2 (Point A in Fig. 6a) with a cloud-top height of 6 km and a τ of 10. When the cloud-top height increased to 14 km, this value changed to 152.1 W/m^2 (Point B in Fig. 6a). This means that the calculated value was lower than the actual value by $\left|\frac{-220.4-(-152.1)}{(-152.1)}\right| \times 100\% = 45\%$ with an underestimate of the cloud-top height by 8 km. When the τ was 90, the 8-km underestimate of cloud-top height underestimated RF by 9.8%. However, the underestimation of cloud-top height had little effect on the RF of the surface, and the error was < 0.1% using the above inputs.

With the increase of the solar zenith angle, the solar radiation to the top of the atmosphere gradually reduces. Under the conditions presented in Fig. 6c, the 8-km underestimation of the cloud-top height underestimated the RF of the Earth system by 46% with a τ of 10. The RF underestimation decreased to 13% with a τ of 90. When the solar zenith angle changed to 60° (Fig. 6e), the rate of RF underestimation increased again.

Compared with a surface consisting of vegetation, an underlying surface of ocean has a different albedo and, therefore, a different impact on RF. As shown in Fig. 6b, d, and f, the underestimation of cloud-top height over the ocean also underestimated the RF of the Earth system. However, the error was less than with a surface of vegetation. For example, assuming the solar zenith angle was 0°, the 8-km underestimate of cloud-top height underestimated the RF of the Earth system by 23% with a τ of 10, and by 7.1% with a τ of 90.

There is no direct solar radiation at night, and the albedo difference will therefore not have an impact on the RF. As shown in Fig. 6g, the clouds mainly played a role in warming the Earth system and the Earth's surface at night. With a τ of 10, the RF of the Earth system was 58.4 W/m^2 with the cloud-top height at 6 km, and 156.9 W/m^2 with the cloud-top height at 14 km, underestimating the correct value by $\left|\frac{58.4-156.9}{156.9}\right| \times 100\% = 63\%$. In contrast to daytime, the underestimation of the cloud-top height also had a certain impact on the Earth's surface RF. For example, the 8-km underestimate of cloud-top height overestimated the Earth's surface RF by 20% with a τ of 10.

The error in RF due to different levels of τ and cloud-top underestimation are shown in Fig. 7 with constant cloud-top underestimation (fixed to 8 km) or constant τ (fixed to 10). In brief, these parameters have a greater impact on the RF of the Earth system than the surface RF. With the increase of underestimation of cloud top, the relative error of the RF also increases.

Therefore, PR-echo-top height for precipitating cloud should be corrected before being the cloud-top height input to simulate the radiative forcing. Although accurate correction might be hard to develop because of the rare near-coincident data, a rough correction was provided in Table 1 based on the percentile of PR, CPR and CALIOP-echo-top heights. For example, if PR-echo-top height is 6.25 km over the land, the CALIOP-cloud-top height will be approximately 15.19 km. Other values can be found or interpolated using the Table.

5. Conclusions

Based on the standard for identifying precipitating cloud, the echo-top height observed by PR, CPR, and CALIOP was analyzed, and the effect of the underestimation of this height on the radiative forcing was simulated by SBDART.

The results show that the PR-echo-top height greatly underestimated the height of the actual precipitating cloud. Regional differences occurred in this underestimation, which was up to 10 km over central Africa, Indonesia, and the American continent. According to Liu and Zipser (2005), tropical convection systems reaching 14 km (tropopause) are defined as overshooting convection. However, the proportion of actual overshooting convection in the tropics is probably much larger than the 1.3% they calculated. Convective activity was inhibited over the Eastern Pacific and the South Atlantic, and therefore the echo-top heights for precipitating cloud observed by PR, CPR, and

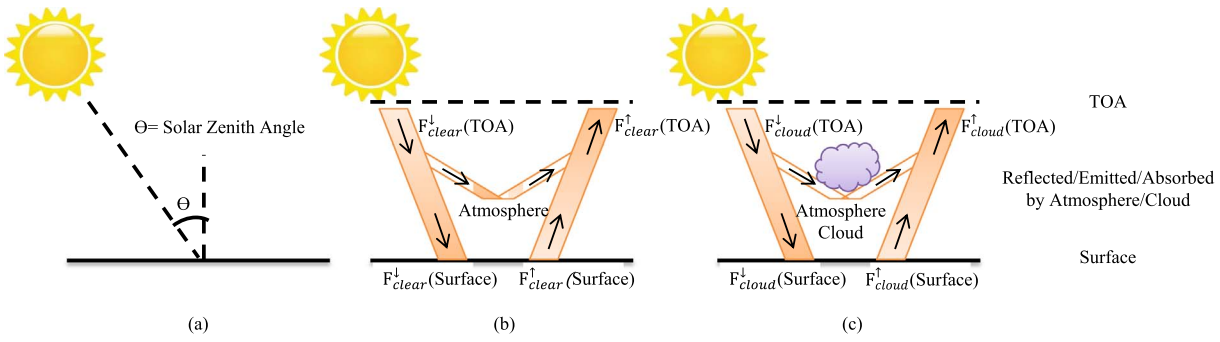

Fig. 5. Schematic diagram of (a) Solar Zenith Angle, (b) $F_{clear}^{\downarrow}$ and $F_{clear}^{\uparrow}$, and (c) $F_{cloud}^{\downarrow}$ and $F_{cloud}^{\uparrow}$. TOA means the top of the atmosphere.

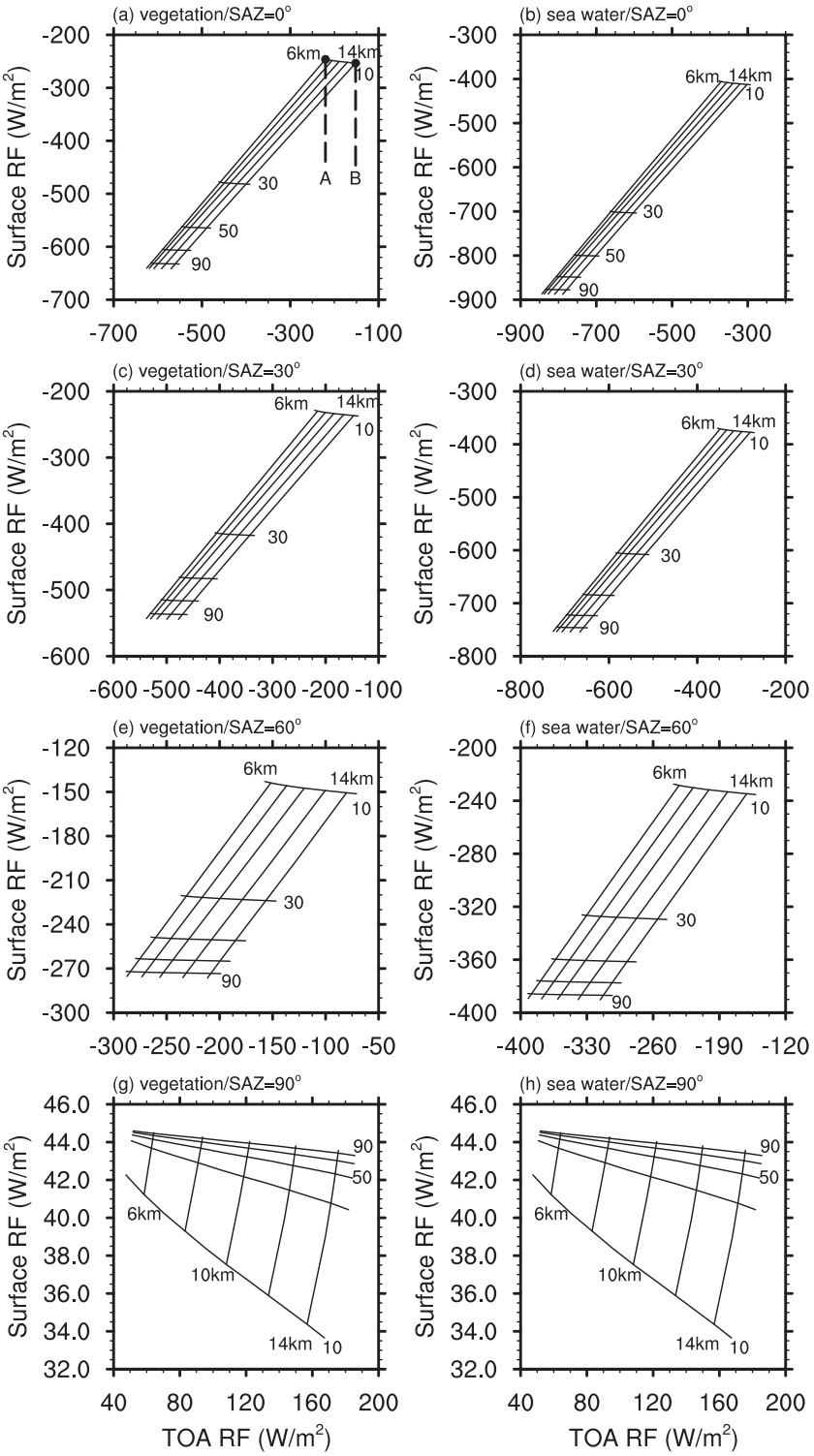

Fig. 6. Influence of the cloud-top height and τ on the RF at the top of the atmosphere (TOA) and the Earth's surface vegetation at a solar zenith angle of (a, b) 0°, (c, d) 30°, (e, f) 60°, and (g, h) 90°.

CALIOP were all located in the trade stable layer (at about 3 km).

The simulation of different cloud-top heights showed that the underestimation of the cloud-top height led to the underestimation of the Earth-system RF with a sun zenith angle of 0°, while it did not have much effect on the RF of the Earth's surface. As τ increased, the effect of the cloud-top underestimation on the Earth-system RF reduced. The relative error of the RF estimation increased with the increase of the sun zenith angle. The underlying surface also influenced the RF underestimate, where the percentage error over land was larger than that over ocean with a constant underestimation of cloud-top height.

Therefore, when using the PR-echo-top height for model inputs or for calculating physical parameters, full consideration should be given to its underestimation of the precipitating-cloud-top height. Appropriate corrections must be applied to different study areas on the basis of the PR-echo-top height to estimate the actual precipitating-cloud-top height.

Acknowledgments

The data can be obtained from the websites http://cloudsat.atmos.

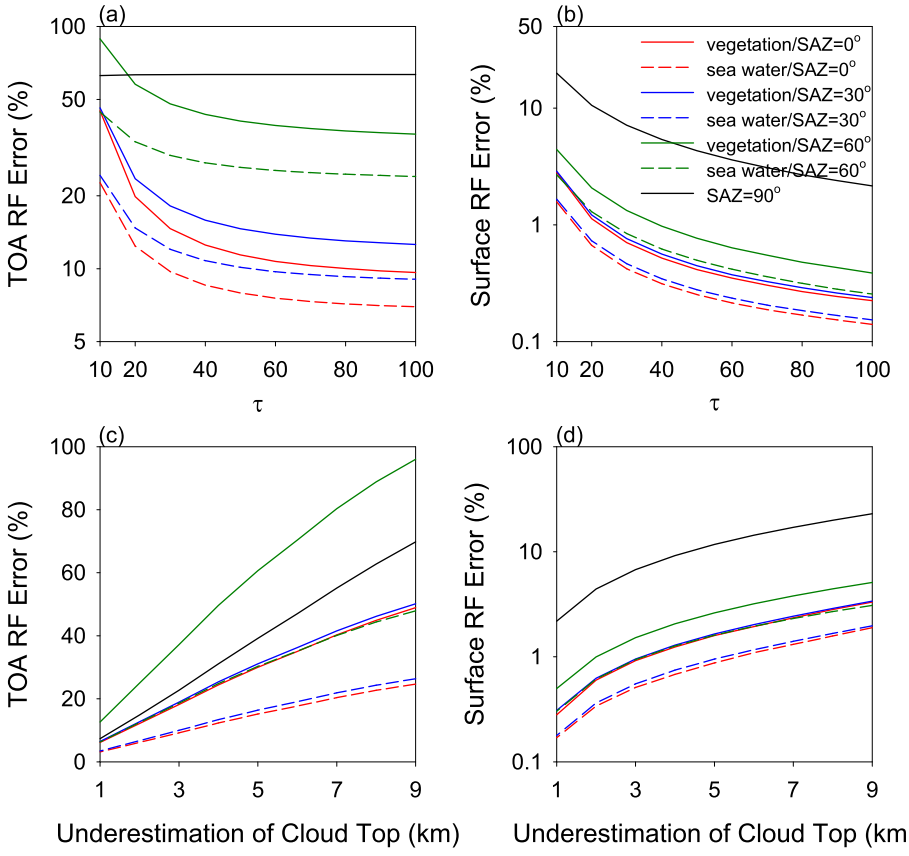

Fig. 7. Relative error of (a) TOA RF and (b) Surface RF as the function of τ with underestimation of cloud top fixed to a constant value (8 km). Relative error of (c) TOA RF and (d) Surface RF as the function of underestimation of cloud top with τ fixed to 10. TOA means the top of the atmosphere. The labels are in connections with panels in Fig. 6. Please note that "SAZ = 90°" represents "vegetation/SAZ = 90°" and "sea water/SAZ = 90°", since albedo difference does not affect the RF.

Table 1
Percentile of the echo-top height for precipitating cloud observed by PR, CPR, and CALIOP over the tropical land and ocean.

	Land (km)			Ocean (km)		
Percentile (%)	PR	CPR	CALIOP	PR	CPR	CALIOP
10	4.00	3.95	6.62	2.75	2.38	2.26
20	5.00	6.26	11.91	3.50	3.34	5.16
30	5.25	8.35	13.68	4.25	5.48	11.76
40	5.75	10.64	14.57	5.00	8.56	13.67
50	6.25	12.02	15.19	5.50	11.45	14.59
60	6.75	12.83	15.68	6.00	12.67	15.23
70	7.25	13.46	16.10	6.75	13.44	15.75
80	8.25	14.09	16.51	7.50	14.12	16.23
90	9.50	14.88	16.99	8.75	14.91	16.76

colostate.edu/data for CPR/CALIOP and https://pmm.nasa.gov/data-access/downloads/trmm for TRMM PR). This work is supported by the National Natural Science Foundation of China (Grants 41230419 and 41675041) and the Special Funds for Public Welfare of China (Grants GYHY201306077 and GYHY201406001).

References

Baker, M.B., 1997. Cloud microphysics and climate. Science 276, 1072–1078.
Casey, S.P.F., Dessler, A.E., Schumacher, C., 2007. Frequency of tropical precipitating clouds as observed by the tropical rainfall measuring mission precipitation radar and ICESat/geoscience laser altimeter system. J. Geophys. Res.-Atmos. 112, D14215.
Chen, Y.L., Fu, Y.F., 2017. Characteristics of VIRS signals within pixels of TRMM PR for warm rain in the tropics and subtropics. J. Appl. Meteorol. Climatol. 56, 789–801.
Chen, F.J., Fu, Y.F., Liu, P., Yang, Y.J., 2016. Seasonal variability of storm top altitudes in the tropics and subtropics observed by TRMM PR. Atmos. Res. 169, 113–126.
Chen, Y.L., Fu, Y.F., Xian, T., Pan, X., 2017. Characteristics of cloud cluster over the steep southern slopes of the Himalayas observed by CloudSat. Int. J. Climatol. 37, 4043–4052. http://dx.doi.org/10.1002/joc.4992.
Fu, Y.F., 2014. Cloud parameters retrieved by the Bispectral reflectance algorithm and associated application. J. Met. Res. 28, 965–982.
Fu, Y.F., Cao, A.Q., Li, T.Y., Feng, S., Zheng, Y.Y., Liu, Y., Zhang, A.M., 2012. Climatic characteristics of the storm top altitude for the convective and stratiform precipitation in summer Asia based on measurements of the TRMM precipitation radar. Acta. Meteor. Sin. 70, 436–451.
Fu, Y.F., Pan, X., Liu, G.S., Li, R., Zhong, L., 2016. Characteristics of precipitation based on cloud brightness temperatures and storm tops in summer over the Tibetan plateau. Chin. J. Atmos. Sci. 40, 102–120.
Fu, Y.F., Zhu, J.C., Yang, Y.J., Yuan, R.M., Liu, G.S., Xian, T., Liu, P., 2017. Grid-cell aerosol direct shortwave radiative forcing calculated using the SBDART model with MODIS and AERONET observations: an application in winter and summer in eastern China. Adv. Atmos. Sci. 34, 952–964.
Fueglistaler, S., Dessler, A.E., Dunkerton, T.J., Folkins, I., Fu, Q., Mote, P.W., 2009. Tropical tropopause layer. Rev. Geophys. 47.
Hamada, A., Takayabu, Y.N., Liu, C.T., Zipser, E.J., 2015. Weak linkage between the heaviest rainfall and tallest storms. Nat. Commun. 6, 6213.
Iguchi, T., Kozu, T., Meneghini, R., Awaka, J., Okamoto, K., 2000. Rain-profiling algorithm for the TRMM precipitation radar. J. Appl. Meteorol. Climatol. 39, 2038–2052.
Im, E., Wu, C.L., Durden, S.L., 2005. Cloud profiling radar for the CloudSat mission. IEEE Aerosp. Electron. Syst. Mag. 20, 15–18.
Johnson, R.H., Rickenbach, T.M., Rutledge, S.A., Ciesielski, P.E., Schubert, W.H., 1999. Trimodal characteristics of tropical convection. J. Clim. 12, 2397–2418.
Kummerow, C., Barnes, W., Kozu, T., Shiue, J., Simpson, J., 1998. The tropical rainfall measuring mission (TRMM) sensor package. J. Atmos. Ocean. Technol. 15, 809–817.
Lau, K.M., Wu, H.T., 2010. Characteristics of precipitation, cloud, and latent heating associated with the Madden-Julian Oscillation. J. Clim. 23, 504–518.
Lau, K.M., Wu, H.T., 2011. Climatology and changes in tropical oceanic rainfall characteristics inferred from tropical rainfall measuring mission (TRMM) data (1998-2009). J. Geophys. Res.-Atmos. 116, D17111.
Li, W., Schumacher, C., 2011. Thick anvils as viewed by the TRMM precipitation radar. J. Clim. 24, 1718–1735.
Liu, C.T., Zipser, E.J., 2005. Global distribution of convection penetrating the tropical tropopause. J. Geophys. Res.-Atmos. 110, D23104.
Liu, C.T., Zipser, E.J., 2009. "Warm rain" in the tropics: seasonal and regional distributions based on 9 yr of TRMM data. J. Clim. 22, 767–779.
Liu, D.Y., Liu, Q., Qi, L., Fu, Y.F., 2016. Oceanic single-layer warm clouds missed by the cloud profiling radar as inferred from MODIS and CALIOP measurements. J. Geophys. Res.-Atmos. 121, 12947–12965.
Mace, G.G., Zhang, Q., 2014. The CloudSat radar-lidar geometrical profile product (RL-GeoProf): updates, improvements, and selected results. J. Geophys. Res.-Atmos. 119, 9441–9462.
Marchand, R., Mace, G.G., Ackerman, T., Stephens, G., 2008. Hydrometeor detection using Cloudsat - an earth-orbiting 94-GHz cloud radar. J. Atmos. Ocean. Technol. 25, 519–533.

Rangno, A.L., Hobbs, P.V., 2005. Microstructures and precipitation development in cumulus and small cumulonimbus clouds over the warm pool of the tropical Pacific Ocean. Q. J. R. Meteorol. Soc. 131, 639–673.
Ricchiazzi, P., Yang, S.R., Gautier, C., Sowle, D., 1998. SBDART: a research and teaching software tool for plane-parallell radiative transfer in the Earth's atmosphere. Bull. Am. Meteorol. Soc. 79, 2101–2114.
Riley, E.M., Mapes, B.E., 2009. Unexpected peak near − 15 °C in CloudSat echo top climatology. Geophys. Res. Lett. 36, L09819.
Sassen, K., Wang, Z., 2007. Level 2 cloud scenario classification product process description and interface control document. http://www.cloudsat.cira.colostate.edu/sites/default/files/products/files/2B-CLDCLASS_PDICD.P_R04.20070724.pdf, Accessed date: 17 July 2016.
Schumacher, C., Houze, R.A., 2003. Stratiform rain in the tropics as seen by the TRMM precipitation radar. J. Clim. 16, 1739–1756.
Schumacher, C., Houze, R.A., 2006. Stratiform precipitation production over sub-Saharan Africa and the tropical East Atlantic as observed by TRMM. Q. J. R. Meteorol. Soc. 132, 2235–2255.
Shige, S., Kummerow, C.D., 2016. Precipitation-top heights of heavy orographic rainfall in the Asian monsoon region. J. Atmos. Sci. 73, 3009–3024.
Stephens, G.L., Vane, D.G., Tanelli, S., Im, E., Durden, S., Rokey, M., Reinke, D., Partain, P., Mace, G.G., Austin, R., L'ecuyer, T., Haynes, J., Lebsock, M., Suzuki, K., Waliser, D., Wu, D., Kay, J., Gettelman, A., Wang, Z., Marchand, R., 2008. CloudSat mission: performance and early science after the first year of operation. J. Geophys. Res.-Atmos. 113, D00A18.
Winker, D.M., Vaughan, M.A., Omar, A., Hu, Y.X., Powell, K.A., Liu, Z.Y., Hunt, W.H., Young, S.A., 2009. Overview of the CALIPSO mission and CALIOP data processing algorithms. J. Atmos. Ocean. Technol. 26, 2310–2323.
Xian, T., Fu, Y.F., 2015. Characteristics of tropopause-penetrating convection determined by TRMM and COSMIC GPS radio occultation measurements. J. Geophys. Res.-Atmos. 120, 7006–7024.
Yang, Y.J., Lu, D.R., Fu, Y.F., Chen, F.J., Wang, Y., 2015. Spectral characteristics of tropical anvils obtained by combining TRMM precipitation radar with visible and infrared scanner data. Pure Appl. Geophys. 172, 1717–1733.
Yang, Y.J., Fu, Y.F., Qin, F., Zhu, J.C., 2017. Radiative forcing of the tropical thick anvils evaluated by combining TRMM with atmospheric radiative transfer model. Atmos. Sci. Lett. http://dx.doi.org/10.1002/asl.74FH6.